CHEMISTRY OF MATERIALS

ARTICLE

pubs.acs.org/cm

Indium Oxide Atomic Layer Deposition Facilitated by the Synergy between Oxygen and Water

Joseph A. Libera, John N. Hryn, and Jeffrey W. Elam*

Energy Systems Division, Argonne National Laboratory, Argonne, Illinois 60439, United States

ABSTRACT: This paper explores the atomic layer deposition (ALD) of indium oxide (In_2O_3) films using cyclopentadienyl indium (InCp) and combinations of both molecular oxygen and water as the co-reactants. When either O_2 or H_2O were used individually as the oxygen source the In_2O_3 growth was negligible over the temperature range 100−250 °C. However, when oxygen and water were used in combination either as a simultaneous exposure or supplied sequentially, In_2O_3 films were deposited at growth rates of 1.0−1.6 Å/cycle over the full range of deposition temperatures. In situ quadrupole mass spectrometry and quartz crystal microbalance measurements revealed that water serves the function of releasing ligands from the surface while oxygen performs the role of oxidizing the indium. Since both processes are necessary for sustained growth, both O_2 and H_2O are required for the In_2O_3 ALD. The electrical resistivity, mobility, and carrier concentration of the In_2O_3 films varied dramatically with both the deposition temperature and co-reactant sequence and correlated to a crystallization occurring at ~140 °C observed by X-ray diffraction and scanning electron microscopy. Using this new process we successfully deposited ALD In_2O_3 films over large area substrates (12 in. × 18 in.) with very high uniformity in thickness and resistivity.

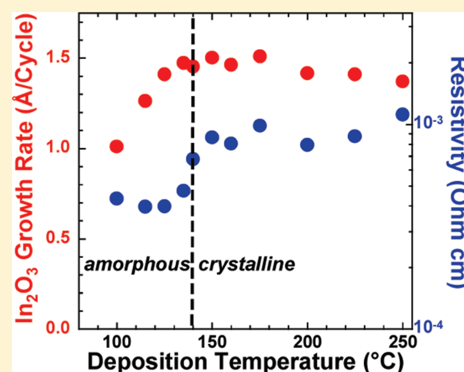

KEYWORDS: atomic layer deposition, indium oxide, resistivity, in situ measurements

INTRODUCTION

Indium−tin oxide (ITO) is one of the most widely used transparent conducting oxides (TCOs) and consists of indium oxide (In_2O_3) doped with approximately 10 atomic % tin oxide. Owing to its excellent combination of high optical transmission, high electrical conductivity, and good chemical stability, ITO thin films are widely used in applications such as flat panel displays, touch screens, solar glass, and energy efficient window coatings.[1,2] Commercial applications of ITO coatings utilize sputtering[3,4] or chemical vapor deposition (CVD)[5−7] to prepare the ITO thin films. However, these deposition techniques suffer from limitations. For instance, it is challenging to achieve precise, uniform coatings using sputtering, and relatively high deposition temperatures are required for CVD. These high temperatures prohibit coating thermally sensitive substrates such as polymers. Furthermore, emerging applications for TCOs based on nano-structured materials demand highly conformal films on porous, high aspect ratio substrates, and this requirement cannot be met by sputtering or CVD. In contrast, atomic layer deposition (ALD) can produce very uniform films with exceptional conformality even on very high aspect ratio substrates. Furthermore, ALD typically allows lower growth temperatures than CVD.

ALD uses alternating exposures to precursor vapors which chemisorb to the substrate surface in a self-limiting manner to deposit films in an atomic layer-by-layer fashion.[8,9] The first demonstrations of In_2O_3 ALD utilized $InCl_3$ as the indium source and either H_2O[10] or hydrogen peroxide[11] as the oxygen source. Although this method produced films with good materials properties,[12−14] relatively high growth temperatures of 400−450 °C were required. Furthermore, the $InCl_3$ precursor was found to etch the deposited In_2O_3 films[10] which prohibits the large precursor exposures necessary to coat porous materials or large area substrates. To circumvent this problem, we developed an alternative method for In_2O_3 ALD utilizing cyclopentadienyl indium (InCp) and ozone (O_3).[15] This method enabled In_2O_3 ALD at temperatures as low as 200 °C without any apparent etching and facilitated the functionalization of nano-porous substrates with ITO to fabricate thin film solar cells.[16,17] In our previous study we also evaluated H_2O, H_2O_2, O_2, and N_2O as potential oxygen sources but found practically no In_2O_3 growth when these precursors were used individually. We hypothesized that only O_3 was a powerful enough oxidant to both strip the ligands from the surface and also oxidize the indium from the +1 to the +3 oxidation state. In_2O_3 ALD has recently been reported using indium(III) acetylacetonate and either H_2O or O_3, but the growth rates were very low and the surface reactions did not appear to be self-limiting.[18]

Although we succeeded in coating high aspect ratio nanoporous substrates using InCp and O_3, we found that thermal decomposition of the O_3 catalyzed by the In_2O_3 reduced the conformality of the In_2O_3 films in high aspect ratio pores and also caused thickness nonuniformities in our ALD reactor producing thinner films downstream of the O_3 injection point.[15] Another limitation of our method was that the minimum growth temperature of 200 °C which appeared to be the threshold

Received: December 21, 2010
Revised: February 23, 2011
Published: March 23, 2011

 © 2011 American Chemical Society

temperature for activating the O_3 prevented us from coating most polymers. Recently we attempted to scale our O_3-based In_2O_3 process from the ~1 in. × 1 in. substrates used in the initial study to a larger substrate size of 12 in. × 18 in. using a cross-flow reactor and found the ozone decomposition problem to be much more severe for these larger substrates. While it may be possible to improve the thickness uniformity using a showerhead to introduce the O_3 more uniformly on the substrate, we were motivated to find a new In_2O_3 ALD process that did not require O_3. We were surprised to discover that when H_2O and O_2 were used in combination, either as a simultaneous exposure (SE) or in the sequence H_2O-O_2 (WO) or O_2-H_2O (OW), very uniform In_2O_3 films were produced on the 12 in. × 18 in. substrates at temperatures as low as 100 °C.

In this manuscript, we describe a detailed examination of In_2O_3 ALD using cyclopentadienyl indium and combinations of water and oxygen as co-reactants in the SE, WO, and OW modes over the temperature range 100−250 °C. Spectroscopic ellipsometry was performed to measure the film thickness, and the structure of the In_2O_3 films was determined by X-ray diffraction (XRD) and scanning electron microscopy (SEM). Hall probe measurements were used to evaluate the electrical transport properties and ultraviolet−visible absorption spectroscopy (UV−vis) was employed to determine the optical transmission. In situ quartz crystal microbalance (QCM) and quadrupole mass spectrometry (QMS) measurements were performed to elucidate the reaction mechanism for the In_2O_3 ALD. To demonstrate some of the advantages of this new process, we prepared uniform ALD In_2O_3 coatings over 12 in. × 18 in. substrates.

EXPERIMENTAL SECTION

Indium oxide films were deposited using a custom ALD viscous flow reactor described previously.[19] The deposition chamber consisted of a stainless steel tube with an inside diameter of 5 cm and a length of 60 cm. Ultrahigh purity nitrogen carrier gas (Airgas 99.998%) continuously flowed through the reactor at 360 sccm and a pressure of 1.1 Torr. Four heated zones maintained a uniform and constant temperature (±3 °C) in the deposition chamber. Cyclopentadienyl indium (InCp, Strem, 99.999%+ electronic grade) was held in a stainless steel bubbler heated to 40−45 °C, and 90 sccm of the N_2 carrier gas was diverted through the bubbler during the InCp exposures. Ultrahigh purity oxygen (Airgas 99.995%) flowing at 200 sccm and water vapor from the head space of a deionized water reservoir were used as oxygen sources for the In_2O_3 ALD. The large area coating experiments utilized a custom cross-flow reactor installed in place of the 5 cm ID flow tube. The large area reactor could accommodate planar substrates with dimensions up to 12 in. × 18 in.

A quartz crystal microbalance (QCM) was used for in situ measurements during the In_2O_3 ALD. The QCM utilized an AT-cut quartz sensor crystal with polished front face (Colorado Crystal Corp. No. CCAT1BK-1007-000) mounted in a Maxtek BSH-150 bakeable sensor head that was modified to prevent deposition on the back of the sensor.[19] The QCM data reported in this paper assumed a bulk density for the In_2O_3 of 7.19 g/cm^3. In situ measurements were also performed using a quadrupole mass spectrometer (QMS, Stanford Research Systems RGA300). The QMS was mounted in a differentially pumped chamber maintained at ~1×10^{-6} Torr by a 50 L/s turbomolecular drag pump and connected to the ALD chamber by a 35 μm orifice.

Conventional metal oxide ALD consists of alternating exposures to a metal precursor, A, and a single oxygen source, B, so that one ALD cycle can be written: A/B. In this study In_2O_3 ALD was performed using combinations of two oxygen sources: oxygen (B1) and water (B2). The In_2O_3 ALD cycles were performed in three ways: simultaneous exposure (SE), A/(B1+B2); oxygen followed by water (OW), A/B1/B2; and water followed by oxygen (WO), A/B2/B1. For comparison, some films were prepared using just water or oxygen. The InCp exposure times were 3 s, and the water and oxygen exposure times were 4 s. Purge times of 5 s were used between each exposure. These exposure times were determined to be saturating, and the purge times were found to be adequate based on in situ QCM measurements.

In_2O_3 films were deposited on Si(100) and fused silica substrates using 300 ALD cycles yielding films of 30−48 nm in thickness. The fused silica substrates were elevated in the deposition chamber to achieve uniform growth on both sides of the substrate which simplified interpretation of the optical transmission measurements. To facilitate prompt and consistent nucleation of the ALD In_2O_3 films, the substrates were first coated with ~2 nm ALD Al_2O_3 using 20 cycles of trimethyl aluminum (Aldrich, 97%) and deionized water with 2 s exposures and 5 s purge periods.

The In_2O_3 film thicknesses were determined from samples prepared on Si(100) substrates using a J.A.Woolam Co. Alpha-SE ellipsometer. We measured the axial uniformity of the In_2O_3 film thickness using multiple Si(100) coupons placed along the 40 cm deposition zone of our ALD reactor and aligned along the direction of precursor flow. Using saturating precursor exposures, we measured a film thickness variation over the 40 cm deposition zone of less than 3%. All of the growth rate values reported in this manuscript were taken from the samples positioned in the middle of the deposition zone. Ultraviolet−visible (UV−vis) optical absorption measurements were performed on the In_2O_3 films prepared on fused silica substrates using a Cary-5000 spectrophotometer.

X-ray diffraction (XRD) measurements were made on a Rigaku Miniflex Plus diffractometer using Cu Kα X-rays. XRD scans were performed on In_2O_3 films prepared on fused silica substrates over the 2θ range 29−39° which encompasses the two strongest diffraction peaks ([400] and [222]) of the cubic In_2O_3 phase. Scanning electron microscopy (SEM) was performed using an Hitachi S4700 with a field emission gun electron beam source. The resistivity, carrier mobility, and carrier concentration were measured using the films prepared on fused silica substrates with an Ecopia HMS-3000 Hall effect measuring system. Before performing the Hall probe measurements, the edges of the fused silica substrates were polished using fine sandpaper to remove the In_2O_3 film and prevent current flow on the opposite side of the substrate which influenced the measurements. The resistivity, mobility, and carrier concentration values reported in this paper are averages of measurements performed on the front and back faces of the fused silica substrates which were always within 5% of each other.

RESULTS AND DISCUSSION

A. Synergistic In_2O_3 Growth Using Water and Oxygen. We first attempted to deposit In_2O_3 on Si(100) substrates using 300 In_2O_3 ALD cycles with only water and oxygen individually as the co-reactants at deposition temperatures of 125, 175, and 225 °C. The purple triangles at the bottom of Figure 1a marked "O" and "W" show the growth rates determined from these samples using spectroscopic ellipsometry. The very low growth rates of 0−0.15 Å/cycle demonstrate that In_2O_3 ALD is negligible under these conditions as expected based on our previous study.[15] Next, a series of In_2O_3 films was prepared on silicon and fused silica substrates over the temperature range 100−250 °C using the three modes for combining the water and oxygen co-reactants: SE, WO, and OW. Remarkably, using water and oxygen together in any of the three modes enabled In_2O_3 deposition at high growth rates of up to 1.6 Å/cycle.

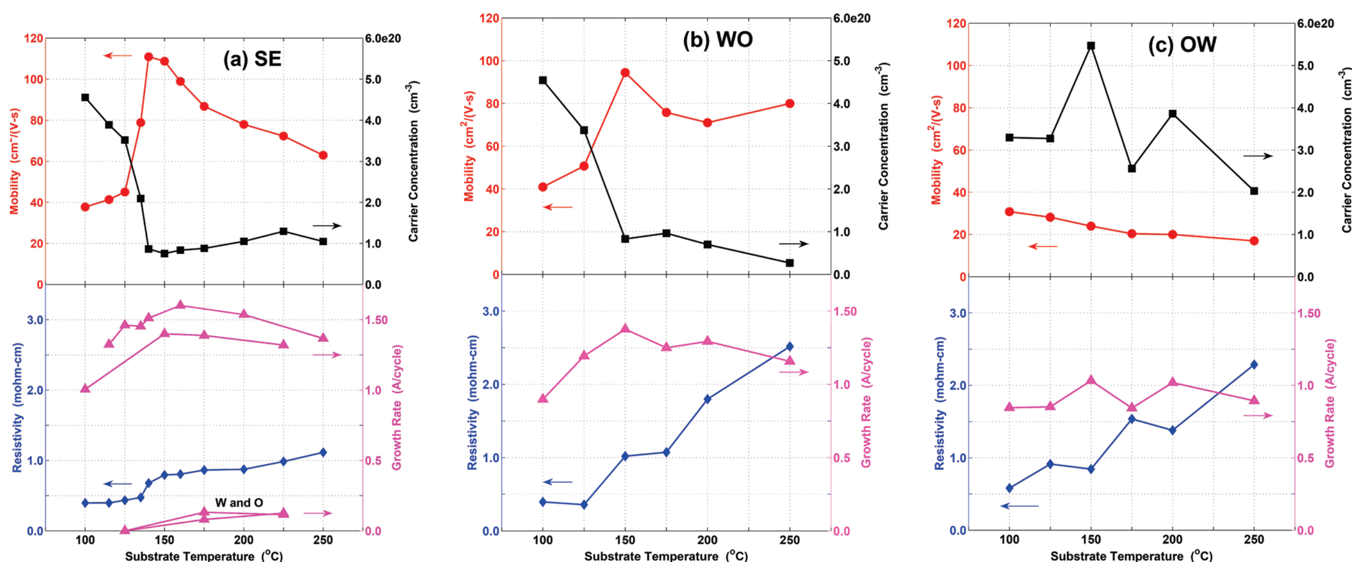

Figure 1. Growth rate determined from spectroscopic ellipsometry (closed triangles), resistivity measured by 4-point probe (closed diamonds), mobility (closed circles) and carrier concentration (closed squares) determined by Hall probe for ALD In_2O_3 films grown using InCp, H_2O, and O_2 using three different growth modes: (a) simultaneous exposure to H_2O and O_2 (SE), (b) H_2O exposure followed by O_2 exposure (WO), and (c) O_2 exposure followed by H_2O exposure (OW). The growth rates given by the solid triangles at the bottom of part (a) result from ALD In_2O_3 films prepared using only O_2 (O) and only H_2O (W) as co-reactants.

The growth rates for the films deposited on Si(100) are indicated by the purple triangles in Figure 1a−c for the SE, WO, and OW modes, respectively. The highest In_2O_3 growth rates were obtained over the entire temperature range using the SE mode. The growth obtained using the WO mode shown in Figure 1b is very similar to that of the SE mode with a maximum at a growth rate of 1.4 Å/cycle at 150 °C. In contrast, the In_2O_3 growth rate for the OW mode is nearly independent of temperature at ∼1.0 Å/cycle. All of the films for Figure 1 were prepared using 3 s InCp exposures with the exception of the lower growth rate curve in Figure 1a which used 2 s InCp exposure times. The In_2O_3 growth rates using 2 s InCp exposures are ∼10% lower than the growth rates obtained using the saturating, 3 s exposures.

B. Transport Properties. Figure 1a−c shows the resistivity (blue diamonds), mobility (red circles), and carrier concentration (black squares) for the SE, OW, and WO modes, respectively, determined from Hall probe measurements of the In_2O_3 films deposited on fused silica. In Figure 1a, the transport properties encompass films prepared using both 2 and 3 s InCp exposures demonstrating that there is no measurable dependence of the transport properties on the exposure time. Although the growth rates changed relatively little with deposition temperature, the transport properties were very sensitive to both the deposition temperature and the deposition mode. Both the SE and the WO modes exhibited a dramatic change in the transport properties near 140 °C. As will be shown below, 140 °C corresponds to the threshold temperature for crystallization of the ALD In_2O_3 films. Most notable for the OW mode is the very low mobility over the entire temperature range. At the lowest deposition temperature of 100 °C, both the SE and the WO modes yielded nearly the same resistivity (ρ = 3.4−3.6 × 10^{-4} Ω·cm), mobility (μ = 38−41 cm/(V·s)), and carrier concentration (n_e = 4.5 × 10^{20} cm^{-3}) while the OW mode gave a slightly higher resistivity and lower mobility and carrier concentration. As the growth temperature increased through the crystallization temperature of 140 °C, the SE mode showed a large jump in mobility from 38 to 111 cm/(V·s) while the carrier concentration dropped to a minimum of 0.8 × 10^{20} cm^{-3}. As the growth temperature was further increased to 250 °C, the mobility in the SE mode steadily declined while for the WO mode this decline reversed and started to increase at the highest temperature. Above 140 °C, both the SE and the WO modes showed a similar carrier density of ∼1 × 10^{20} cm^{-3}. The resistivity in the SE mode showed two essentially constant values, below and above the crystallization temperature, whereas the resistivity of the WO mode increased steadily above the crystallization temperature. The transport properties of films prepared using the OW mode showed a very low mobility over the entire temperature range in contrast with the SE and WO modes. The carrier concentration stayed relatively high and the resistivity showed a similar trend to the WO mode. Possible explanations for these changes in transport properties with growth temperature and growth mode will be discussed in Section D below after we consider the In_2O_3 crystallinity.

The In_2O_3 films prepared using both O_2 and H_2O as co-reactants in the SE mode were analyzed by UV−vis spectrophotometry. For these measurements, In_2O_3 films were deposited on both sides of the quartz substrates yielding effective thicknesses of 600−950 Å. In the visible and near-infrared spectral region between 400 and 1100 nm, the average transmittance of these samples was in the range of T = 80−87%. These values are slightly lower than the values of T = 90% and T = 95% measured previously for ALD In_2O_3 films prepared using InCp/O_3 and $InCl_4/H_2O$, respectively.[10,16] The lower transmittance values in the present investigation might result from a higher concentration of oxygen vacancies since our films are also more conducting than those in the former studies.

C. In_2O_3 Crystallinity. Figure 2a−c shows the results of XRD measurements for the In_2O_3 films prepared on Si(100) substrates and reveals a distinct crystallization behavior that is common to each of the three modes. All of the films were

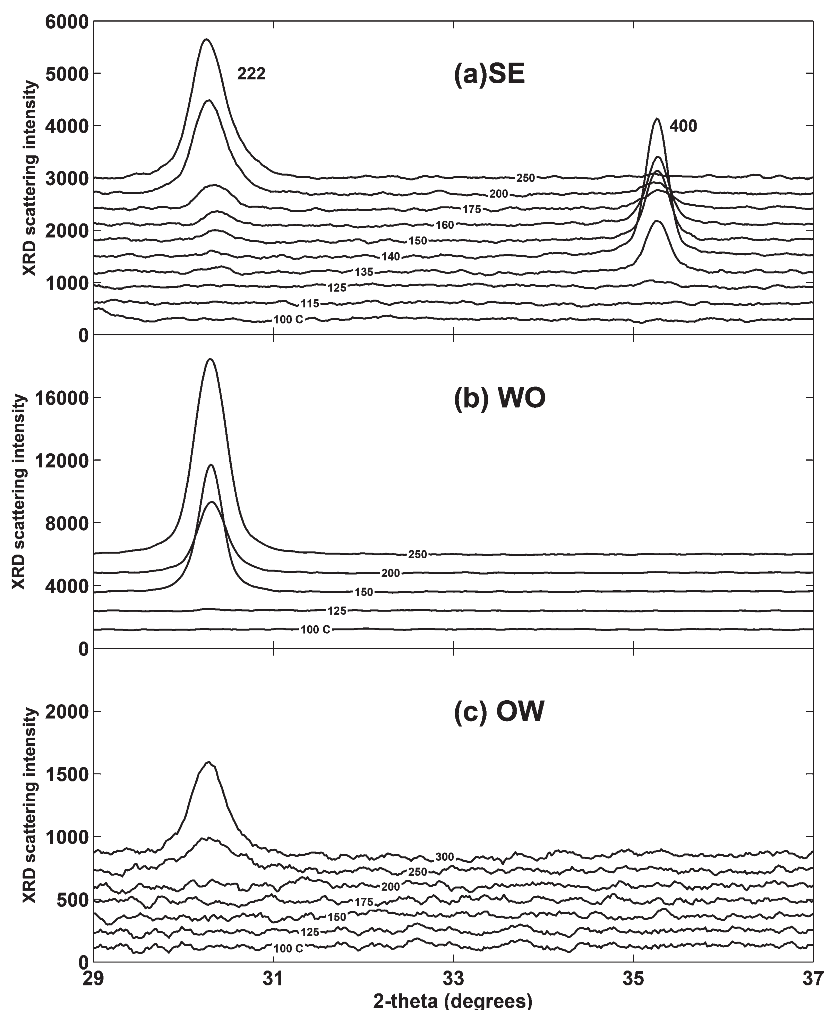

Figure 2. X-ray diffraction measurements for ALD In_2O_3 films prepared on Si(100) substrates versus deposition temperature using the growth modes SE (a), WO (b), and OW (c).

amorphous at deposition temperatures < 130 °C, and crystallization started at 135 °C. The OW and WO modes gave films that were highly textured along the [222] direction while the SE mode films exhibited a relatively strong [400] texture near the crystallization temperature of ~135 °C which then changed to the [222] texture at higher deposition temperatures. The lowest degree of crystallization occurred in the OW films where the [222] diffraction peak first occurred at a deposition temperature of 250 °C. This contrasts the WO mode where crystallization began at ~150 °C. At 250 °C, the magnitude of the [222] diffraction peak for the WO mode is 12 000 compared to 2600 for the SE mode and only 750 for the OW mode. Scanning electron microscope (SEM) images of the SE mode film prepared at 175 °C (Figure 3) showed surface features consistent with crystalline domains of several hundred nanometers. In contrast, SEM images of the SE mode film prepared at 100 °C (not shown) were completely featureless suggesting an amorphous film. Our results are in general agreement with previous reports that thin In_2O_3 films deposited at low temperatures (30−160 °C) exhibit an amorphous to crystalline transition at ~150 °C.[20,21] However, in some cases even amorphous, low temperature In_2O_3 films exhibit low resistivity indicating that crystallinity is not a prerequisite for high conductivity.[22,23]

D. Structure Property Relationships. It is well-known that the larger crystal domains characteristic of more highly crystalline materials can provide a higher mobility as a result of reduced carrier scattering at grain boundaries. But at the same time, larger domains can lower conductivity by decreasing the number of intrinsic charge carriers provided by defects at the grain boundaries. To compensate for this effect, In_2O_3 films are typically doped extrinsically with tin to form ITO and generate carrier sites which persist when the films are annealed to increase the crystal size and improve the mobility.

In the present study, the lowest resistivities were found for the amorphous films in which the relatively large carrier concentration dominated the low mobility imparted by the amorphous state. With increasing deposition temperature in both the SE and WO series films, the carrier concentration plummeted and the mobility rose rapidly leaving the resistivity nearly constant. This compensating behavior is explained by increased crystallization (Figure 2) that enhances the mobility at the expense of charge carriers which are probably oxygen vacancies. Beyond the crystallization temperature of ~140 °C, the mobility generally declined with increasing temperature. While this seems to contradict the notion that higher temperatures yield more crystalline films with higher mobilities, it is likely in our case that the higher

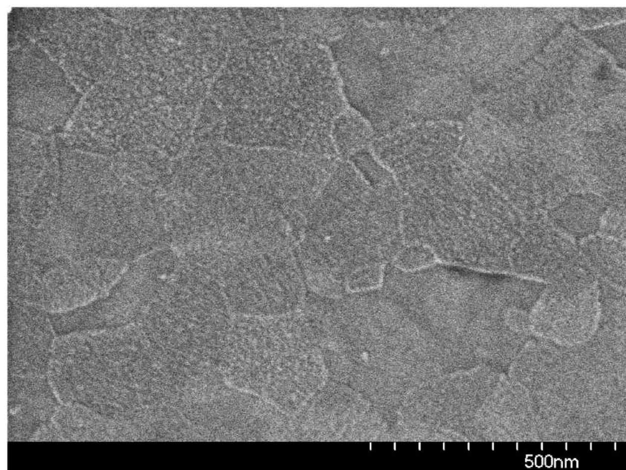

Figure 3. Scanning electron micrograph of ALD In_2O_3 film prepared on fused silica substrate at 175 °C using the SE growth mode.

temperatures generated an increased number of individual crystallites. This notion is consistent with the faster nucleation seen by QCM at higher growth temperatures (Figure 6 and Section F below) and also with the relatively steady carrier concentration observed in the range 150−250 °C. The exception to this trend is the 250 °C WO sample where a high mobility of 80 cm/(V·s) was observed which is the largest mobility measured for films prepared at this temperature. The 250 °C WO sample also exhibited the strongest [222] peak in XRD. In the SE series however, we saw a steady decline in mobility from 140 °C onward and the mobility for the OW series was distinctly lower than for the other modes. These findings suggest that the presence of water during the final step in the ALD cycle may influence the In_2O_3 crystallinity and electrical transport properties.

E. In Situ QMS and QCM Studies. To explore the mechanism for the In_2O_3 ALD as well as the nucleation of In_2O_3 films on Al_2O_3 surfaces, simultaneous QMS and QCM measurements[15,16,24,25] were performed during the In_2O_3 ALD at 125 and 175 °C for each of the three deposition modes. These temperatures were selected to be below and above the amorphous-to-crystalline transition temperature of 150 °C to detect any possible changes in growth mechanism from the crystallization. In addition to the combined QCM/QMS data sets acquired at 125 and 175 °C, QMS data were gathered during In_2O_3 ALD at a range of temperatures up to 250 °C. Without exception, the predominant reaction product observed by QMS was cyclopentadiene at mass-to-charge ratio m/e = 66. Previous in situ QMS measurements of In_2O_3 ALD using InCp and O_3 identified CO_2 at m/e = 44 as the major gas phase reaction product during the O_3 exposures.[15] However, we did not observe any m/e = 44 product signals in the present study using O_2 and H_2O as the co-reactants.

The in situ QCM-QMS measurements were performed by first depositing ALD Al_2O_3 onto the QCM crystal using alternating exposures to TMA and H_2O until the Al_2O_3 growth rate settled to a constant value of 1.0 Å/cycle for at least 20 cycles. This procedure ensured that the surface of the QCM crystal was sufficiently flat to avoid artifacts due to surface area enhancement from surface roughness. Furthermore, the ALD Al_2O_3 provided a chemically uniform starting surface so that the nucleation of the In_2O_3 ALD could be monitored.

QCM-QMS data sets of 60−70 ALD cycles were recorded for each growth mode and temperature. These data sets were then processed to generate averaged profiles of the QCM and QMS data during steady-state growth and transient growth rate data from the start of the growth experiment to examine the nucleation behavior. To generate the average steady-state cycle profiles, the final 10 cycles of the 60−70 cycle data sets were averaged. Figure 4a,b shows the growth profiles measured at 125 and 175 °C, respectively, for all three growth modes. The m/e = 66 QMS peaks for the averaged profiles were quantitatively analyzed by first subtracting the background signals and then integrating to determine the peak areas. The background QMS signals were obtained by interrupting the steady state growth and performing multiple exposures to either InCp alone or to the co-reactants (H_2O and/or O_2) alone. The background signals originated from sources such as cracking of the InCp precursor in the QMS and residual cyclopentadiene in the InCp reservoir.

Referring to Figure 4a,b, the following characteristics are common to all of the deposition modes and temperatures: (1) Cyclopentadiene is released from the InCp-terminated surface only during the water exposures. (2) During the water exposures, the mass gains and the m/e = 66 peak heights are inversely related. In fact, there is a slight *decrease* in mass during the water exposure for the OW mode at 175 °C which also shows the largest m/e = 66 peak. (3) The oxygen exposures always yield approximately the same mass increase regardless of the deposition mode or temperature. (4) No gas phase product is released during the oxygen exposures.

We postulate that the In_2O_3 ALD occurs according to the following overall reaction:

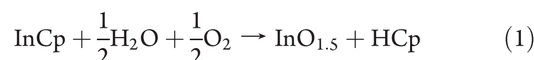

$$\mathrm{InCp} + \frac{1}{2}\mathrm{H_2O} + \frac{1}{2}\mathrm{O_2} \rightarrow \mathrm{InO_{1.5}} + \mathrm{HCp} \quad (1)$$

Equation 1 can be divided into the following three steps:

(A)

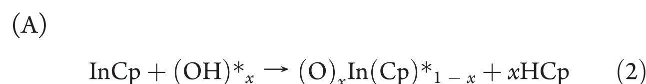

$$\mathrm{InCp} + (\mathrm{OH})^*_x \rightarrow (\mathrm{O})_x\mathrm{In}(\mathrm{Cp})^*_{1-x} + x\mathrm{HCp} \quad (2)$$

(B)

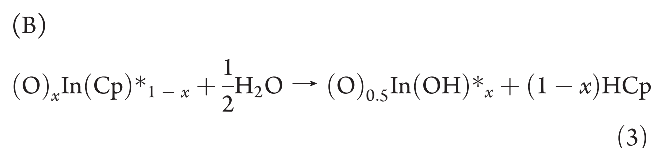

$$(\mathrm{O})_x\mathrm{In}(\mathrm{Cp})^*_{1-x} + \frac{1}{2}\mathrm{H_2O} \rightarrow (\mathrm{O})_{0.5}\mathrm{In}(\mathrm{OH})^*_x + (1-x)\mathrm{HCp} \quad (3)$$

(C)

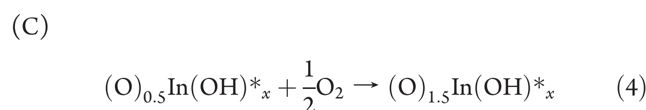

$$(\mathrm{O})_{0.5}\mathrm{In}(\mathrm{OH})^*_x + \frac{1}{2}\mathrm{O_2} \rightarrow (\mathrm{O})_{1.5}\mathrm{In}(\mathrm{OH})^*_x \quad (4)$$

In eqs 1−4, HCp represents cyclopentadiene, the asterisks denote surface species, and all other species are in the gas phase. In step (A), InCp reacts with x surface hydroxyl groups (where x may be temperature- and/or mode-dependent) to liberate x Cp ligands leaving $(1 - x)$ Cp ligands on the surface. In step (B), H_2O reacts with the resulting surface to release the remaining $(1 - x)$ Cp ligands and regenerate the initial hydroxyl coverage. Note that after the completion of step (B) the indium remains in a low oxidation state (e.g., +1 as in the InCp compound). In step (C), the indium is oxidized by O_2 to the +3 oxidation state, and

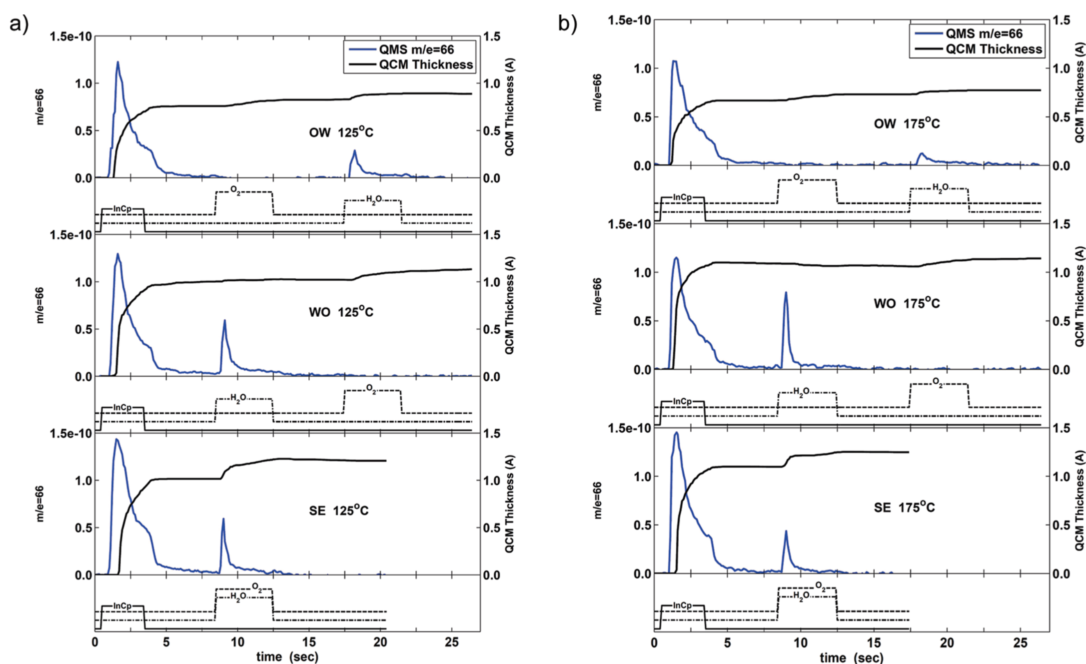

Figure 4. In situ QCM and QMS measurements recorded during In_2O_3 ALD at 125 °C (a) and 175 °C (b). Each data trace is an average over 10 cycles and represents the transient signal observed during individual In_2O_3 ALD cycles using the OW (top panel), WO (middle panel), and SE (bottom panel) growth modes. The solid blue lines show the QMS signals at m/e = 66 for the InCp species in arbitrary units and the solid black lines show the QCM thickness measurements in Å/cycle. The black traces below each panel designate the exposures to InCp (solid), O_2 (dashed), and H_2O (dot-dashed).

the expected $InO_{1.5}$ stoichiometry is achieved. In this mechanism, the H_2O and O_2 each perform separate but necessary functions: the H_2O liberates the Cp ligands and rehydroxylates the surface while the O_2 oxidizes the indium. Consequently, steps (B) and (C) can occur in either order (OW, WO) or they can occur together during a simultaneous exposure (SE) but both steps are required for growth. Although the mechanism proposed is speculative, in the following discussion we will demonstrate that all of the in situ measurements are consistent with the mechanism described by eqs 1−4.

To analyze the data in Figure 4a,b more quantitatively, we can define some additional parameters as illustrated in Figure 5. The net mass gain for a complete ALD cycle is G, while ΔM_A and ΔM_B are the mass changes resulting from the first and second precursor exposure steps, respectively. The ratios $R_A = G/(\Delta M_A)$ and $R_B = G/(\Delta M_A + \Delta M_B)$ are dimensionless parameters to characterize the relative mass gains after completion of the A and B steps, respectively. The quantity R_A can be used to evaluate the fraction of Cp ligands, x, released upon adsorption of InCp on the surface:

$$R_A = m(InO_{1.5})/[m(InCp) - xm(HCp)] \quad (5)$$

where the m values refer to the molecular weights of the corresponding species. As the fraction of ligands released varies from $x = 0$ (no ligand release) to $x = 1$ (complete ligand release), R_A will vary from 0.77 to 1.21.

Table 1 lists the quantities calculated from the in situ QCM and QMS measurements in Figure 4a,b. In this table, A_{66} is the total integrated m/e = 66 QMS signal for one complete ALD cycle while $A_{66,InCp}$ and $A_{66,H2O}$ are the fractions of the m/e = 66 signal observed during the InCp and H_2O exposures, respectively. G_{QCM} is the In_2O_3 ALD growth rate determined from the QCM measurements while G_{film} is the corresponding growth

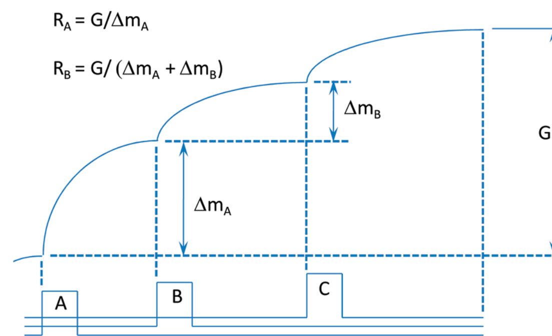

Figure 5. Schematic diagram illustrating structure of QCM traces resulting from exposures to the three precursors A, B, and C and defining the quantities G, ΔM_A, ΔM_B, and the ratios $R_A = G/(\Delta M_A)$ and $R_B = G/(\Delta M_A + \Delta M_B)$.

rate determined from the ex situ spectroscopic ellipsometry measurements performed on Si(100) substrates. G_{QCM}/A_{66} is the ratio of these two quantities normalized to the average value, R_A and R_B are the QCM step ratios defined in Figure 5, and x is calculated from eq 5. The numbers shown in parentheses in Table 1 are the predicted values for R_B.

Table 1 shows that the R_A values are in the range 1.04−1.16. No systematic trends are seen in the R_A values with either the deposition mode or the temperature, and in fact the values are all nearly identical with the exception of the WO value at 175 °C which appears to be an outlier. This consistency suggests that a similar In_2O_3 ALD mechanism applies under all of these conditions. The fraction of ligands released during the InCp adsorption deduced from the QCM measurements, x, is in the range 0.70−0.92. These values can be compared to the fraction of m/e = 66 signals observed in the QMS during the InCp exposures,

Table 1. Quantities Derived from the in Situ QCM and QMS Measurements during In_2O_3 ALD Performed at 125 and 175°C Using the SE, WO, and OW Modes[a]

	125 °C			175 °C		
	SE	WO	OW	SE	WO	OW
A_{66}	2.58×10^{-9}	2.14×10^{-9}	1.57×10^{-9}	2.18×10^{-9}	1.81×10^{-9}	1.46×10^{-9}
$A_{66,InCP}$	0.83	0.73	0.84	0.85	0.72	0.88
$A_{66,H2O}$	0.17	0.27	0.16	0.15	0.28	0.12
G_{film}	1.46	1.19	0.87	1.4	1.25	0.84
G_{QCM}	1.21	1.13	0.89	1.25	1.14	0.77
G_{QCM}/A_{66}	0.85	0.96	1.03	1.05	1.15	0.96
R_A	1.16	1.16	1.15	1.14	1.04	1.15
R_B	n/a	1.11 (1.13)	1.08 (1.08)	n/a	1.08 (1.13)	1.05 (1.08)
x	0.91	0.91	0.89	0.88	0.70	0.89

[a] A_{66} is the total integrated QMS signal at $m/e = 66$ for one complete ALD cycle while $A_{66,InCp}$ and $A_{66,H2O}$ are the fractions of the $m/e = 66$ signals observed during the InCp and H_2O exposures, respectively. G_{QCM} is the In_2O_3 ALD growth rate determined from the QCM measurements while G_{film} is the corresponding growth rate determined from the ex situ spectroscopic ellipsometry measurements performed on Si(100) substrates. G_{QCM}/A_{66} is the ratio of these two quantities normalized to their average value while R_A and R_B are the QCM step ratios described in the text and shown in Figure 5. The quantities shown in parentheses are the predicted values for R_B as described in the text. The quantity x is the fraction of Cp ligands released during the InCp adsorption.

A_{66InCp}, which are in the range 0.72−0.88. The close similarity between the QCM and QMS values lends confidence to both measurements and supports the assertion that cyclopentadiene is the only significant gas phase product during the In_2O_3 ALD.

The R_B values in Table 1 allow us to evaluate the hypothesis that the oxygen exposures serve the function of oxidizing the indium. During the O_2 exposures in the WO growth mode, no Cp ligands remain on the surface and one oxygen atom is adsorbed so we expect that

$$R_B = m(InO_{1.5})/m(InO_{0.5}) = 1.13 \quad (6)$$

Table 1 shows that the R_B values for the WO mode are 1.11 and 1.08 at 125 and 175 °C, respectively, in very good agreement with the predicted value of 1.13. During the O_2 exposures of the OW growth mode, some Cp ligands remain on the surface so that

$$R_B = m(InO_{1.5})/[m(InCp) - xm(HCp) + m(O)] \quad (7)$$

The R_B values for the OW growth mode in Table 1 are 1.08 and 1.05 at 125 and 175 °C, respectively. The value calculated from eq 7 for both growth temperatures using the appropriate values for x is $R_B = 1.08$ in very good agreement with the experimental values. Consequently, the QCM measurements confirm the mechanism presented in eqs 1−4, and in particular these measurements support the notion that O_2 serves the function of fully oxidizing the indium.

The G_{QCM} values in Table 1 were deduced from the in situ QCM measurements assuming a bulk In_2O_3 density of 7.19 g/cm^3. Table 1 shows fairly good agreement between the G_{QCM} values and the G_{film} growth rates determined using ex situ spectroscopic ellipsometry lending confidence to both sets of measurements. With the exception of the OW measurement at 125 °C, the G_{QCM} values are consistently lower than the G_{film} values by 8−17% suggesting that the In_2O_3 density may be lower than the bulk value. This finding is not surprising given that XRD shows the films to be amorphous or weakly crystalline in this temperature range. The G_{QCM}/A_{66} values in Table 1 list the ratio of these quantities normalized to their average value. These values are all close to unity and range from 0.85 and 1.15 indicating that the A_{66} quantities determined from the in situ QMS measurements are also a reliable indicator of the In_2O_3 growth. In addition, the agreement between the QCM and QMS values further argues that Cp is the only major gas phase product from the In_2O_3 ALD.

Although our model for the In_2O_3 growth using H_2O and O_2 is consistent with all of the measurements, the true growth mechanism is likely to be more complex. For instance, the observation that not all of the Cp ligands were released during the InCp exposures suggests additional sites for InCp adsorption besides surface hydroxyls. These sites are likely to be labile surface oxygen. In addition, we recorded subtle changes in growth rate and more pronounced changes in crystallinity and electrical transport properties depending on the order in which the H_2O and O_2 were introduced, and these changes are not captured by our model. Additional in situ techniques such as infrared spectroscopy to identify the surface species and X-ray absorption spectroscopy to determine the indium oxidation state may help to refine the model and explain these behaviors.

F. Nucleation of In_2O_3 on Al_2O_3. The results described thus far pertain to In_2O_3 growth in the steady-state. However, the QCM measurements in this study were all initiated on an ALD Al_2O_3 surface, and this affords the opportunity to examine the nucleation phase of the In_2O_3 ALD. Figure 6 plots the In_2O_3 growth rate vs cycles measured by QCM. For both the 125 and the 175 °C cases, an induction period was observed in the In_2O_3 growth. The initial growth rate was very low but climbed steadily with increasing In_2O_3 ALD cycles and passed through a maximum before decreasing and leveling off to a steady-state value. This phenomenon is usually attributed to the formation and coalescence of islands where the growth initiates only at discrete surface sites.[26] As the In_2O_3 islands expand in three dimensions, the surface area grows and pushes the In_2O_3 growth rate above the steady-state value. As the islands coalesce to form a continuous film, the surface area returns to normal causing the growth rate to decrease and approach the steady-state value. It is very interesting that at both temperatures the nucleation behavior is nearly identical for each of the three growth modes in the initial stages. Only in the later stages do the growth rates diverge for the different growth modes and approach their respective

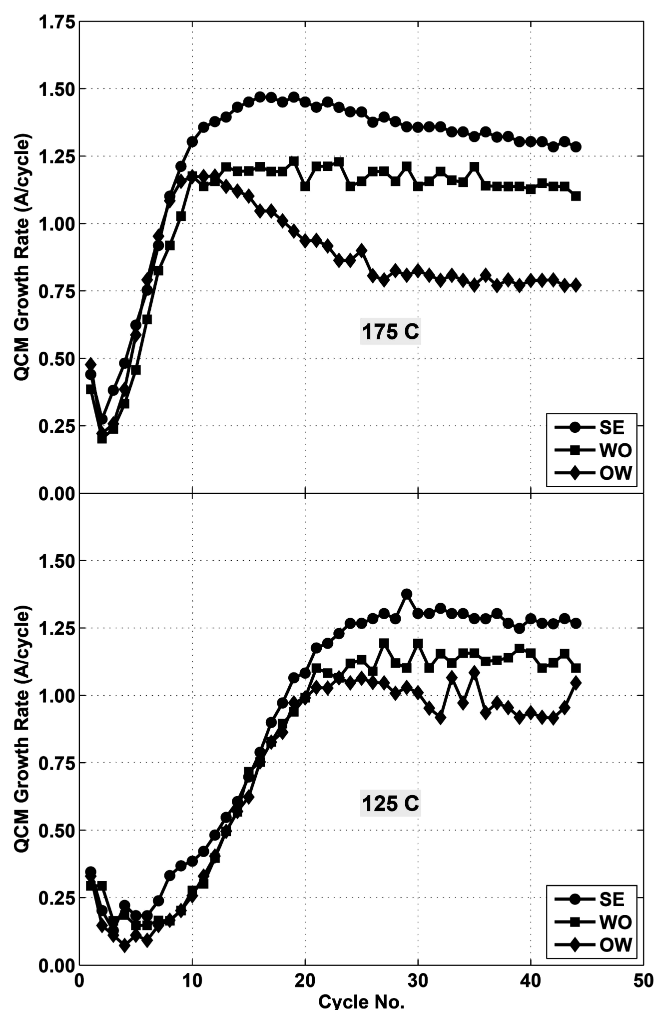

Figure 6. In_2O_3 growth rates versus number of ALD cycles when starting on an Al_2O_3 surface at 125 °C (bottom panel) and 175 °C (top panel) for the SE (circles), WO (squares), and OW (diamonds) growth modes as determined from QCM measurements.

steady-state values. The growth rate for the very first In_2O_3 ALD cycle is higher than for the subsequent cycles, and this reflects the density of nucleation sites on the Al_2O_3 surface. This value is smaller at the lower growth temperature, and consequently 20 cycles are required to reach the maximum growth rate at 125 °C while only 10 cycles are needed at 175 °C. It is likely that the longer incubation times at lower growth temperatures will produce rougher In_2O_3 films in analogy with previous QCM measurements during tungsten ALD.[27]

G. ALD In_2O_3 over Large Area Substrates. To evaluate the potential for scaling up our In_2O_3 ALD processes to bigger substrates, we developed a large area, hot-walled chamber able to accommodate planar substrates with dimensions of up to 12 in. × 18 in. This large area chamber substitutes in place of the tubular deposition chamber on our existing ALD reactor. We first used the InCp/ozone process[15] to deposit In_2O_3 films with a thickness of ~20 nm on 8 in. × 8 in. glass plates and obtained thickness variations of up to ±100% with the thickness tapering off in the axial dimension downstream of the precursor injection point and laterally toward the edges of the substrate. We attributed these thickness variations to ozone thermal decomposition catalyzed by the In_2O_3.[15] Next, we used 158 cycles of InCp/H_2O/O_2 in the WO mode to coat Si(100) substrates spanning the 12 in. × 18 in. dimensions of the large area reactor and obtained the thickness profile shown in Figure 7. These films are very uniform and exhibited a thickness standard deviation of only 2.5%. The resistivity for films prepared under similar conditions on 8 in. × 8 in. glass plates was also very uniform at 2.74 mΩ·cm with a standard deviation of 6.0%. These results are very encouraging for the future scale up of In_2O_3-containing films by ALD using the InCp/H_2O/O_2 process.

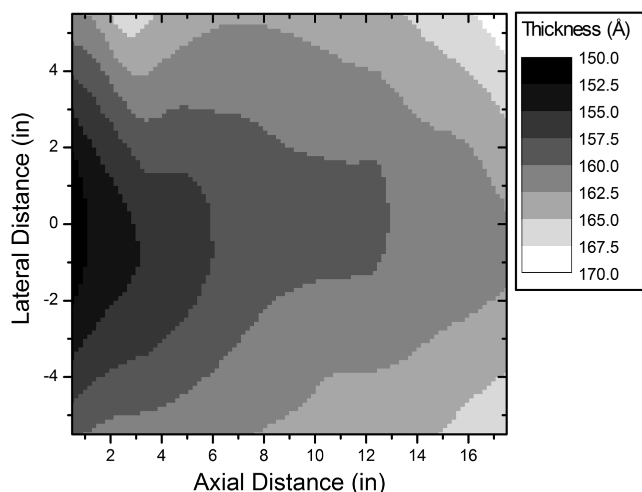

Figure 7. In_2O_3 film thickness resulting from 158 In_2O_3 ALD cycles in the OW mode measured using spectroscopic ellipsometry for silicon substrates covering an area of 18 in. × 12 in. in the large area chamber. Axial distance is along the gas flow direction and lateral distance is perpendicular to the flow.

CONCLUSIONS

This study explored In_2O_3 ALD using InCp and combinations of both O_2 and H_2O as the co-reactants. No In_2O_3 growth occurred when O_2 or H_2O were used alone. However, when O_2 and H_2O were used together or in sequence, In_2O_3 films were deposited at growth rates of 1.0−1.6 Å/cycle over the full range of deposition temperatures from 100 to 250 °C. The In_2O_3 deposited in an amorphous state at temperatures below ~125 °C but became more crystalline for higher growth temperatures. The preferred In_2O_3 orientation and the electrical properties depended on both the temperature and the co-reactant sequence. Furthermore, changes in the In_2O_3 mobility and carrier concentration could be correlated with the changes in crystallinity observed by XRD. In situ QCM and QMS measurements revealed an In_2O_3 growth mechanism in which H_2O serves the function of releasing ligands from the surface while O_2 performs the role of oxidizing the indium. Since both processes are necessary for sustained growth, both O_2 and H_2O are required for the In_2O_3 ALD. Furthermore, QCM measurements showed that the In_2O_3 nucleation on Al_2O_3 surfaces proceeds by island coalescence. Finally, we successfully deposited In_2O_3 films using the InCp/H_2O/O_2 process over large area substrates with very high uniformity in the thickness and resistivity.

AUTHOR INFORMATION

Corresponding Author

*E-mail: jelam@anl.gov.

■ ACKNOWLEDGMENT

This work was supported by the U.S. Department of Energy, EERE-Solar Energy Technologies Program under FWP-4911A. The in situ analysis was supported as part of the Argonne-Northwestern Solar Energy Research (ANSER) Center, an Energy Frontier Research Center funded by the U.S. Department of Energy, Office of Science, Office of Basic Energy Sciences under Award Number DE-SC0001059. Electron microscopy was performed at the Electron Microscopy Center for Materials Research (EMCMR) at Argonne National Laboratory. Use of the EMCMR was supported by the U.S. Department of Energy, Office of Science, Office of Basic Energy Sciences, under Contract No. DE-AC02-06CH11357 operated by UChicago Argonne, LLC.

■ REFERENCES

(1) Edwards, P. P.; Porch, A.; Jones, M. O.; Morgan, D. V.; Perks, R. M. *Dalton Trans.* **2004**, *19*, 2995–3002.
(2) Lewis, B. G.; Paine, D. C. *MRS Bull.* **2000**, *25* (8), 22–27.
(3) Qiao, Z.; Latz, R.; Mergel, D. *Thin Solid Films* **2004**, *466* (1−2), 250–258.
(4) Nishimura, E.; Ohkawa, H.; Song, P. K.; Shigesato, Y. *Thin Solid Films* **2003**, *445* (2), 235–240.
(5) Ni, J.; Yan, H.; Wang, A. C.; Yang, Y.; Stern, C. L.; Metz, A. W.; Jin, S.; Wang, L.; Marks, T. J.; Ireland, J. R.; Kannewurf, C. R. *J. Am. Chem. Soc.* **2005**, *127* (15), 5613–5624.
(6) Kim, H. W.; Kim, N. H.; Myung, J. H. *J. Mater. Sci.* **2005**, *40* (18), 4991–4993.
(7) Kim, N. H.; Myung, J. H.; Kim, H. W.; Lee, C. *Phys. Status Solidi A* **2005**, *202* (1), 108–112.
(8) Ritala, M.; Leskela, M. . In *Handbook of Thin Film Materials*; Nalwa, H. S., Ed.; Academic Press: San Diego, 2001; Vol. 1, p 103.
(9) George, S. M. *Chem. Rev.* **2010**, *110* (1), 111–131.
(10) Asikainen, T.; Ritala, M.; Leskela, M. *J. Electrochem. Soc.* **1994**, *141* (11), 3210–3213.
(11) Ritala, M.; Asikainen, T.; Leskela, H. *Electrochem. Solid State Lett.* **1998**, *1* (3), 156–157.
(12) Asikainen, T.; Ritala, M.; Leskela, M. *Vacuum* **1995**, *46* (8−10), 887–887.
(13) Asikainen, T.; Ritala, M.; Leskela, M. *J. Electrochem. Soc.* **1995**, *142* (10), 3538–3541.
(14) Asikainen, T.; Ritala, M.; Leskela, R.; Prohaska, T.; Friedbacher, G.; Grasserbauer, M. *Appl. Surf. Sci.* **1996**, *99* (2), 91–98.
(15) Elam, J. W.; Martinson, A. B. F.; Pellin, M. J.; Hupp, J. T. *Chem. Mater.* **2006**, *18* (15), 3571–3578.
(16) Elam, J. W.; Baker, D. A.; Martinson, A. B. F.; Pellin, M. J.; Hupp, J. T. *J. Phys. Chem. C* **2008**, *112* (6), 1938–1945.
(17) Martinson, A. B. F.; Elam, J. W.; Liu, J.; Pellin, M. J.; Marks, T. J.; Hupp, J. T. *Nano Lett.* **2008**, *8* (9), 2862–2866.
(18) Nilsen, O.; Balasundaraprabhu, R.; Monakhov, E. V.; Muthukumarasamy, N.; Fjellvag, H.; Svensson, B. G. *Thin Solid Films* **2009**, *517* (23), 6320–6322.
(19) Elam, J. W.; Groner, M. D.; George, S. M. *Rev. Sci. Instrum.* **2002**, *73* (8), 2981–2987.
(20) Paine, D. C.; Whitson, T.; Janiac, D.; Beresford, R.; Yang, C. O.; Lewis, B. *J. Appl. Phys.* **1999**, *85* (12), 8445–8450.
(21) Bellingham, J. R.; Phillips, W. A.; Adkins, C. J. *J. Phys.: Condens. Matter* **1990**, *2* (28), 6207–6221.
(22) Walsh, A.; Da Silva, J. L. F.; Wei, S. H. *Chem. Mater.* **2009**, *21* (21), 5119–5124.
(23) Graham, M. R.; Adkins, C. J.; Behar, H.; Rosenbaum, R. *J. Phys.: Condens. Matter* **1998**, *10* (4), 809–819.
(24) Juppo, M.; Rahtu, A.; Ritala, M.; Leskela, M. *Langmuir* **2000**, *16*, 4034–4039.
(25) Rahtu, A.; Alaranta, T.; Ritala, M. *Langmuir* **2001**, *17*, 6506–6509.
(26) Puurunen, R. L. *Chem. Vap. Deposition* **2003**, *9* (5), 249–257.
(27) Wind, R. W.; Fabreguette, F. H.; Sechrist, Z. A.; George, S. M. *J. Appl. Phys.* **2009**, *105* (7), 074309.